Observed regional impacts of marine heatwaves on air-sea CO_2 exchange

Catherine Li[1,2], Friedrich A. Burger[1,2], Christoph C. Raible[1,2] and Thomas L. Frölicher[1,2]

[1]Climate and Environmental Physics, Physics Institute, University of Bern, Bern, Switzerland.
[2]Oeschger Centre for Climate Change Research, University of Bern, Bern, Switzerland.

Key Points:

- Marine heatwaves substantially affect local air-sea CO_2 fluxes via oceanic pCO_2 changes, but their global impacts remains minor.
- During MHWs, tropics decrease outgassing from lower DIC, while mid latitudes weaken uptake due to thermally induced rise in oceanic pCO_2.
- MHW events can trigger extreme CO_2 flux anomalies, notably in the eastern equatorial Pacific, Indian Ocean and Northeast Pacific.

Corresponding author: Thomas L. Frölicher, `thomas.froelicher@unibe.ch`

Abstract

Marine heatwaves (MHWs) have devastating effects on ecosystems and impact regional air-sea CO_2 exchange. Yet a global assessment of these regional impacts of MHWs on the air-sea CO_2 exchange is missing. Here, we analyze thirty global observation-based air-sea CO_2 flux datasets from 1990 to 2019. We observe minimal reduction in global oceanic CO_2 uptake during MHWs. Regional variations are evident with the equatorial Pacific experiencing a 31% (spread across datasets: 3–49%) reduction in carbon release, suggesting that MHWs are the dominant drivers of strong air-sea CO_2 flux anomalies in this region. In low-to-mid latitudes, MHWs cause a 29% (19–37%) decrease in air-sea CO_2 uptake. Reduced dissolved inorganic carbon in the tropics weakens outgassing, while high ocean temperatures diminish uptake in the low-to-mid latitudes. In the North Pacific and Southern Ocean, enhanced carbon uptake occurs during MHWs, but uncertainties in pCO_2 datasets limit a comprehensive assessment in these regions.

Plain language summary

Periods of unusually warm sea surface temperatures have recently been shown to impact the exchange of carbon dioxide between the surface ocean and overlying atmosphere. We find that extremely warm sea surface temperatures (marine heatwaves) have a small impact on the ocean's overall ability to take up carbon dioxide from the atmosphere, but depending on the region the local exchange of carbon dioxide between the ocean and atmosphere can be substantially impacted. In tropical regions, the ocean's usual release of carbon dioxide to the atmosphere is reduced during marine heatwaves due to lower dissolved inorganic carbon in the surface ocean. In low to mid latitude regions, the ocean's uptake of carbon from the atmosphere is reduced during marine heatwaves due to the effect of warmer temperatures. A clear consensus on the impact of marine heatwaves in the North Pacific and Southern Ocean does not emerge due to data limitations. While heatwaves in the ocean can cause substantial changes in air-sea carbon dioxide exchange in some tropical areas and the Northeast Pacific, they are not the main reason for large monthly changes in globally integrated air-sea carbon dioxide exchange.

1 Introduction

Human-induced carbon dioxide (CO_2) emissions are the primary driver of climate change (IPCC, 2021), with the ocean playing a crucial role in mitigating global warming by taking up about a quarter of these emissions (Friedlingstein et al., 2023). An accurate quantification and understanding of the variability of air-sea CO_2 fluxes is essential for predicting future climate trends (Joos et al., 1999) and assessing the ocean ecosystem response (Gattuso et al., 2015).

In recent decades, prolonged periods of anomalously warm sea surface temperatures, known as marine heatwaves (MHWs; Pearce and Feng (2013); Hobday et al. (2016)), have occurred across all ocean basins (Frölicher & Laufkötter, 2018; Oliver et al., 2021), posing substantial risks to marine species, ecosystems and ecosystem services (Collins et al., 2019; Cheung & Frölicher, 2020; Hughes et al., 2017; Smale et al., 2019; Cheung et al., 2021). With global ocean warming, MHWs are becoming more frequent, intense, and prolonged (Oliver et al., 2018; Frölicher et al., 2018). Individual MHWs are generated by a combination of local oceanic and atmospheric processes including air-sea heat flux, horizontal and vertical temperature advection, and vertical mixing (Vogt et al., 2022; Bian et al., 2023), and are often associated with large-scale climate phenomena such as the El Niño Southern Oscillation (Oliver et al., 2021; Holbrook et al., 2019).

Recent research has highlighted the significance of MHWs in influencing regional oceanic pCO_2 and air-sea CO_2 fluxes (Arias-Ortiz et al., 2018; Mignot et al., 2022; Duke et al., 2023; Edwing et al., 2024). For example, Mignot et al. (2022) identified reduced oceanic

CO_2 release in the equatorial Pacific and decreased oceanic CO_2 uptake around 40°N in the North Pacific. Duke et al. (2023) examined the North Pacific subpolar gyre, revealing substantial anomalous oceanic uptake of CO_2 during recent MHWs due to limited wintertime entrainment and therefore lower oceanic pCO_2. Additionally, Arias-Ortiz et al. (2018) suggested significant carbon release from seagrass carbon stocks to the atmosphere following the Western Australia 2011 MHW. Despite these insights, a comprehensive global assessment of MHWs impacts on air-sea CO_2 fluxes and their driving mechanisms is lacking. Moreover, understanding how CO_2 flux anomalies during MHWs compare to overall flux variability remains limited, hindering a comprehensive evaluation of the importance of MHWs for air-sea CO_2 flux variability.

In this study, we explore the impacts of MHW events on air-sea CO_2 exchange. Using an ensemble of observation-based pCO_2 and wind products spanning from 1990 to 2019, we initially assess the global and regional impacts of MHW events on air-sea CO_2 fluxes. Subsequently, we identify the underlying mechanisms driving flux anomalies during MHWs. Finally, we contextualize these anomalies within the broader spectrum of natural CO_2 flux variability to assess their relative significance in total regional CO_2 flux variability.

2 Methods

2.1 Observation-based data

To identify MHWs, we use the global observation-based daily-mean sea surface temperature (SST) data from the National Oceanic and Atmospheric Administration (NOAA; Daily Optimum Interpolation Sea Surface Temperature OISST dataset v2.1, Huang et al., 2021). This comprehensive dataset combines in situ ship and buoy sea surface temperature observations with satellite-derived measurements from the Advanced Very High-Resolution Radiometer. Through interpolation, data gaps are filled to create a spatially and temporally complete representation of sea surface temperature. To ensure consistency with the CO_2 flux and oceanic pCO_2 data, the daily mean SST data is regridded from $0.25^\circ \times 0.25^\circ$ to $1^\circ \times 1^\circ$ and averaged from daily to monthly-mean values, spanning the period 1982 to 2021.

For the assessment of CO_2 flux anomalies during MHWs, we rely on CO_2 flux estimates derived from the SeaFlux version 2021.04 ensemble data product (Fay et al., 2021). This dataset integrates six global observation-based pCO_2 products, all based on the Surface Ocean Carbon Dioxide Atlas (SOCAT) pCO_2 dataset (Bakker et al., 2016), alongside five global wind reanalyses (Supporting Information Tables S1 and S2). Combined, we obtain 30 distinct air-sea CO_2 flux datasets at monthly intervals, covering the period 1990 to 2019 on a $1^\circ \times 1^\circ$ grid. We only analyze CO_2 flux data in regions where data from all six observation-based pCO_2 products are available.

To analyze the drivers of CO_2 flux anomalies during MHWs, we use the LIARv2 alkalinity regression algorithm (Carter et al., 2018). This algorithm utilizes salinity data from the Hadley Centre (EN4.2.2; Good et al., 2013) in conjunction with sea surface temperature data to compute total alkalinity on a $1^\circ \times 1^\circ$ grid. Dissolved Inorganic Carbon (DIC) is then calculated with CO2SYS (Humphreys et al., 2022) using the estimated total alkalinity, pCO_2 from the six different SeaFlux pCO_2 data products, temperature, salinity, and monthly mean climatologies of phosphate and silicate from the World Atlas 2018 (WOA18; Boyer et al., 2018; Garcia et al., 2019).

2.2 MHW definition and air-sea CO_2 flux anomalies

A MHW is identified when the local linearly detrended monthly-mean SST surpasses the local seasonally-varying 90th percentile of SST. The seasonally varying 90th percentile is calculated for each calendar month separately and is based on linearly detrended monthly-mean SST data spanning from 1982 to 2021. The threshold is set to capture extreme temperature anomalies while ensuring a sufficiently large sample size of MHW months for robust statistical analyses. In contrast to the prevailing approach in MHW studies (Hobday et al., 2016; Le Grix et al., 2021), we define MHWs here on monthly anomalies rather than daily anomalies to be consistent with temporal resolution of the CO_2 flux products.

We calculate the monthly mean air-sea CO_2 flux anomalies during MHWs by initially linearly detrending the air-sea CO_2 flux over the period 1990 to 2019. Subsequently, the anomalies during MHWs are derived as deviations from the climatological seasonal cycle of monthly-mean CO_2 fluxes during MHWs.

We divide the global ocean into eight study regions (Figure 1a, and Supporting Information Table S3) given the diverse characteristics of air-sea CO_2 flux, such as strong or weak CO_2 sink or source regions. To assess whether the product-ensemble-mean air-sea CO_2 flux during MHWs significantly differs from the mean CO_2 flux, we conduct a standard two-sample t-test globally and for each study region, using the 5% significance level (Wilks, 2019).

2.3 Decomposition of air-sea CO_2 flux anomalies into drivers

To determine the driving mechanisms behind the air-sea CO_2 flux anomalies during MHWs, we conduct a first-order Taylor series decomposition of the air-sea flux components. This analysis allows us to quantify the contribution of the solubility, gas transfer velocity, oceanic pCO_2, and atmospheric pCO_2 to the overall air-sea CO_2 flux anomaly during MHWs.

SeaFlux computes the net air-sea CO_2 flux ($F_{air-sea}$) via the adapted bulk formula established by Wanninkhof (1992):

$$F_{air-sea} = k_w \cdot sol \cdot (\mathrm{pCO_{2,a}} - \mathrm{pCO_{2,o}}), \tag{1}$$

where k_w is the gas transfer velocity (in units m s^{-1}), sol is the solubility of CO_2 in seawater (mol m$^{-3}\mu$atm^{-1}), $pCO_{2,a}$ represents the partial pressure of atmospheric CO_2 in the marine boundary layer (μatm), and $pCO_{2,o}$ is the partial pressure of surface ocean CO_2 (μatm). Note that the bulk formula is adapted to omit sea ice regions as not all data products encompass these regions.

The first order Taylor series decomposition of the air-sea CO_2 flux anomalies during MHWs (referred to hereafter as $\Delta F_{air-sea}$) is as follows:

$$\begin{aligned}\Delta F_{\text{air-sea}} \approx & \underbrace{\frac{\partial F_{\text{air-sea}}}{\partial k_{\text{w}}} \cdot \Delta_{k_{\text{w}}}}_{k_w \text{ term}} + \underbrace{\frac{\partial F_{\text{air-sea}}}{\partial sol} \cdot \Delta_{sol}}_{sol \text{ term}} + \underbrace{\frac{\partial F_{\text{air-sea}}}{\partial \mathrm{pCO_{2,o}}} \cdot \Delta_{\mathrm{pCO_{2,o}}}}_{\mathrm{pCO_{2,o}} \text{ term}} \\ & + \underbrace{\frac{\partial F_{\text{air-sea}}}{\partial \mathrm{pCO_{2,a}}} \cdot \Delta_{\mathrm{pCO_{2,a}}}}_{\mathrm{pCO_{2,a}} \text{ term}}\end{aligned} \tag{2}$$

The right hand side of equation (2) represents the contributions of the gas transfer velocity, solubility, and oceanic and atmospheric partial pressure of CO_2. The delta values represent the mean anomalies of the variables during MHWs and the partial derivatives are calculated with the temporal mean values.

The oceanic pCO_2 anomalies are further decomposed as:

$$\Delta \mathrm{pCO}_{2,o} \approx \underbrace{\frac{\partial \mathrm{pCO_{2,o}}}{\partial \mathrm{DIC}} \cdot \Delta_{\mathrm{DIC}}}_{p\mathrm{CO_{2,o}^{DIC}} \text{ term}} + \underbrace{\frac{\partial \mathrm{pCO_{2,o}}}{\partial \mathrm{ALK}} \cdot \Delta_{\mathrm{ALK}}}_{\mathrm{pCO_{2,o}^{ALK}} \text{ term}} + \underbrace{\frac{\partial \mathrm{pCO_{2,o}}}{\partial T} \cdot \Delta_{T}}_{\mathrm{pCO}_{2,o}^{T} \text{ term}} + \underbrace{\frac{\partial \mathrm{pCO_{2,o}}}{\partial S} \cdot \Delta_{S}}_{\mathrm{pCO}_{2,o}^{S} \text{ term}} \tag{3}$$

where oceanic $pCO_{2,o}$ is a function of sea surface dissolved inorganic carbon (DIC), alkalinity (ALK), temperature (T), and salinity (S). The 'mocsy 2.0' Fortran 95 routine (Orr & Epitalon, 2015) is used to calculate the partial derivatives, evaluated at temporal mean values for S, T, DIC, ALK, phosphate, and silicate.

3 Results

3.1 Global and regional response of air-sea CO_2 fluxes during MHWs

Globally, we observe a small reduction in the oceanic uptake of CO_2 by an average of -0.04 mol C/m^2/yr during MHWs, with values ranging from 0.01 (anomalous uptake) to -0.11 mol (anomalous release) C/m^2/yr depending on the dataset used (Figure 1b). This reduction corresponds to approximately 8% (3 to 19%) of the net global oceanic uptake of CO_2 during the time period from 1990 to 2019. In most regions, the CO_2 flux - whether into or out of the ocean in the climatological mean - is diminished during MHWs. Consequently, the air-sea CO_2 flux anomaly pattern during MHWs is reversed from the climatological mean CO_2 flux pattern (Figure 1a).

Although the global CO_2 flux response during MHWs is minor, we observe substantial CO_2 flux responses on the regional scale. The CO_2 uptake in the North Atlantic and the low-mid latitude regions in both the northern and southern hemispheres is reduced by an average of -0.10 mol C/m^2/yr (-0.24 to -0.00), -0.17 mol C/m^2/yr (-0.22 to -0.11), and -0.12 mol C/m^2/yr (-0.18 to -0.04), respectively. In the equatorial Pacific, CO_2 outgassing is reduced by an average of 0.30 (0.03 to 0.48) mol C/m^2/yr. However, this general pattern of reduced air-sea CO_2 fluxes does not apply to the North Pacific and the Southern Ocean. In these regions, CO_2 uptake is even stronger during MHWs (North Pacific: 0.14 (-0.12 to 0.30); Southern Ocean: 0.09 (-0.05 to 0.22) mol C/m^2/yr). In the equatorial Atlantic and the equatorial Indian Ocean, MHW events have minimal to no effect on the air-sea CO_2 fluxes.

The spread in the air-sea CO_2 flux anomalies during MHWs across all observation-based products is considerable (Figure 1b). The primary contributors to this spread are the pCO_2 datasets, as indicated by the contrast between the purple and black ranges in Figure 1b. Minimal variation is observed between CO_2 flux anomalies calculated with the average pCO_2 product and different wind products (not shown), further underscoring the role of pCO_2 reconstructions as the primary source of uncertainty. As a result, significant CO_2 flux anomalies during MHW are only detectable in four of the eight study regions: the equatorial Pacific, the low-to-mid latitudes in both hemispheres, and the Southern Ocean. While statistical significant changes are observed in the Southern Ocean, a comprehensive assessment is hindered by the absence of the pCO_2 data, particularly during austral winter (Landschützer et al., 2016; Gray et al., 2018).

3.2 Drivers of air-sea CO_2 flux changes during MHWs

To detect the drivers of air-sea CO_2 flux changes during MHWs we apply the Taylor decomposition to all air-sea flux components on global scale as well as for all regions. Note that the analysis of regions and globally, which do not show a significant response of the air-sea CO_2 flux during MHWs, helps to understand compensating processes and assessing the origin of the uncertainty.

At the global scale, all components of the air-sea CO_2 flux (gas transfer velocity, solubility, oceanic and atmospheric pCO_2; Equation (2)) collectively contribute to the reduced uptake of CO_2 by the ocean during MHWs (Figure 2a). Oceanic $pCO_{2,O}$ experiences a slight increase during MHWs, leading to an average reduction of air-sea CO_2 flux by -0.012 mol C m^{-2} yr^{-1}. However, there is considerable variability across data products, ranging from -0.052 mol C m^{-2} yr^{-1} to positive contributions of 0.051 mol C

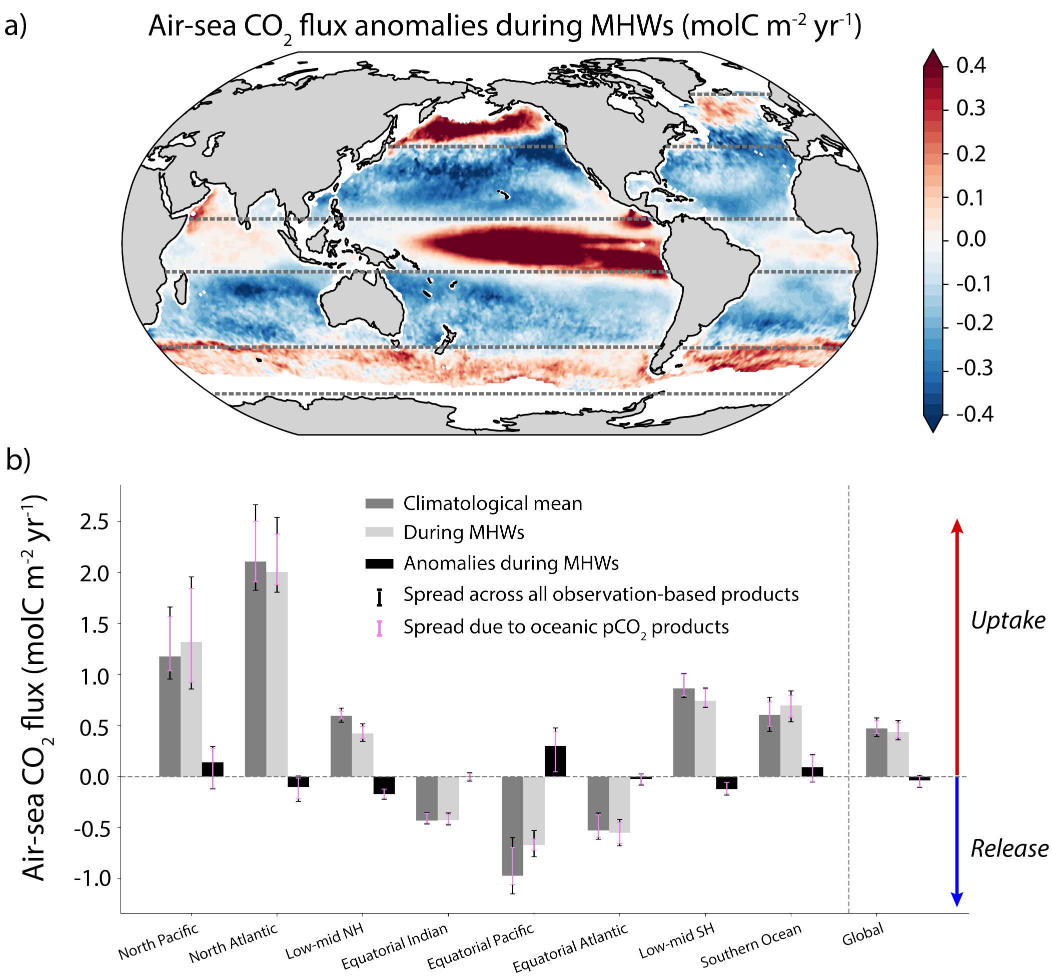

Figure 1. a) Observation-based air-sea CO_2 flux anomalies during MHWs averaged over the 1990-2019 period and across all observation-based products. Data is only shown for regions where all six observation-based pCO_2 products have data. The grey dashed lines indicate the regions shown in panel b). b) Climatological mean air-sea CO_2 flux, mean air-sea CO_2 flux during MHWs and mean air-sea CO_2 flux anomalies during MHWs for the years 1990-2019. The bars represent the averages across all observation-based products. The black error lines represent the min-max spread across the 30 observation-based data products. The purple error lines represent the min-max spread originating from the six observation-based pCO_2 products using the average wind product.

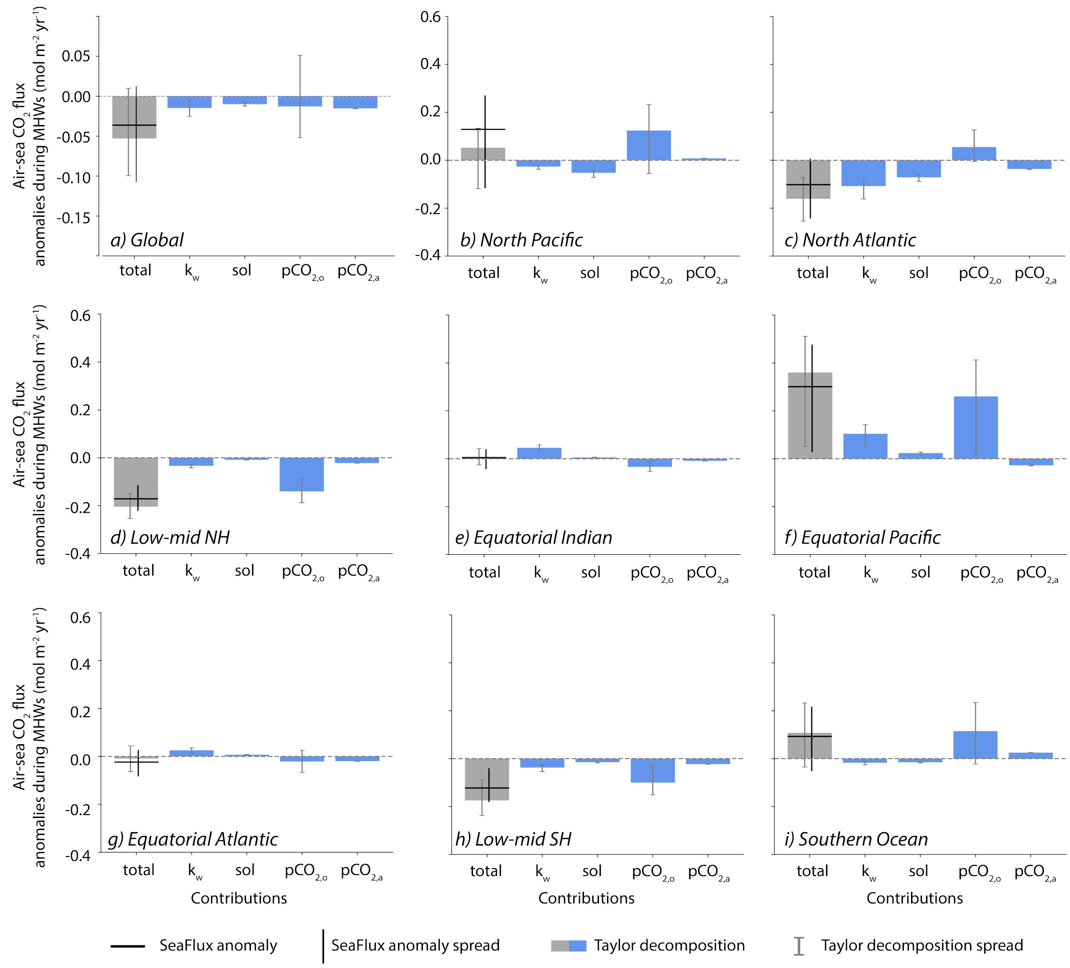

Figure 2. Global and regional drivers of air-sea CO_2 flux anomalies during MHWs over the 1990-2019 period across all observation-based products. The blue bars represent the average contribution of each flux term to the air-sea CO_2 flux anomalies during MHWs with grey error bars representing the min-max spread across the 30 observation-based data products. The grey bar is the sum of all the contribution terms. For comparison, the horizontal black line is the averaged observation-based product air-sea CO_2 flux anomalies during MHWs, and the black error lines represent the min-max spread across the 30 observation-based data products. A positive contribution indicates anomalous uptake, while a negative contribution suggests anomalous outgassing.

m^{-2} yr^{-1}. Decreased wind speed, and consequently gas transfer velocity, during MHWs results in a negative contribution of -0.015 (-0.025 to -0.004) mol C m^{-2} yr^{-1} to the air-sea CO_2 flux. Moreover, the global decrease in solubility due to warmer sea surface temperatures as well as lower atmospheric $pCO_{2,a}$ during MHWs, also contribute negatively, with values of -0.010 (-0.013 to -0.008) mol C m^{-2} yr^{-1} and -0.015 (-0.016 to -0.015) mol C m^{-2} yr^{-1}, respectively.

When analyzing the different regions individually (Figure 2b-i; Supplementary Figure S1), oceanic $pCO_{2,o}$ changes emerge as the primary driver of air-sea CO_2 flux anomalies during MHWs in most regions. Notably, regions such as the North Pacific (Figure 2b), the equatorial Pacific (Figure 2f) and the Southern Ocean (Figure 2i) experience anomalously lower oceanic $pCO_{2,o}$ (i.e., a positive $pCO_{2,o}$ contribution), leading to increased air-sea CO_2 fluxes during MHWs. Conversely, the low-mid latitudes in both hemisphere (Figure 2d,h) experience higher oceanic $pCO_{2,O}$ (i.e., a negative $pCO_{2,O}$ contribution) and therefore lower air-sea CO_2 fluxes during MHWs.

The secondary driver of air-sea CO_2 flux anomalies varies across regions. In the equatorial Pacific (Figure 2f), anomalous CO_2 uptake is also substantially driven by weaker gas transfer velocities during MHWs (i.e. weaker winds). In the North Pacific (Figure 2b), reduced solubility and weaker gas transfer velocities somewhat offset the stronger uptake. In the North Atlantic (Figure 2c), the anomalous outgassing is caused by a combination of weaker gas transfer velocities and lower solubility, which reduce the region's ability to uptake CO_2 and outweigh the decrease in $pCO_{2,O}$ observed during MHWs. In the equatorial Indian (Figure 2e) and Atlantic Ocean (Figure 2g), the very small CO_2 flux anomalies during MHWs are a result of small and counterbalancing contributions of changes in oceanic $pCO_{2,O}$ and the gas transfer velocities. The atmospheric $pCO_{2,a}$ changes play a negligible role in all regions.

By breaking down the oceanic $pCO_{2,O}$ anomalies during MHWs (Equation (3)), we can attribute the flux response to a balance between thermal (temperature) and non-thermal dissolved inorganic carbon (DIC) effects on oceanic $pCO_{2,O}$ (Figure 3), along with changes in alkalinity and salinity. In all ocean regions, the thermal effect - resulting from elevated sea surface temperatures during MHWs - positively contributes to oceanic $pCO_{2,O}$ anomalies. Globally, this effect increases oceanic $pCO_{2,O}$ by 15.34 (15.24 to 15.39) μatm. This is due to the decrease in CO_2 solubility in seawater and due to an increase in CO_2 concentration from a shift in chemical equilibrium between carbonate species with rising temperatures, both leading to anomalously higher oceanic $pCO_{2,O}$. Simultaneously, lower DIC concentrations during MHWs result in anomalously lower oceanic $pCO_{2,O}$ of -18.12 (-19.11 to -16.16) μatm. Changes in alkalinity contribute to a small increase in oceanic $pCO_{2,O}$ and salinity changes are negligible at the global scale.

While globally, the thermal and DIC effects on oceanic $pCO_{2,O}$ nearly balance each other out (Figure 3a), the dominance of either effect varies by region (Figure 3b-i; Supplementary Figure S2). In the equatorial Pacific (Figure 3f) and high latitude regions like the North Pacific (Figure 3b), North Atlantic (Figure 3c), and Southern Ocean (Figure 3i), the decrease in oceanic $pCO_{2,O}$ anomalies driven by DIC outweighs the increase caused by thermal effects. This DIC-driven effect is particularly notable in the equatorial Pacific, where it counteracts both thermal and alkalinity-driven $pCO_{2,O}$ increases during MHWs, resulting in lower than usual $pCO_{2,O}$ (-8.43 (-12.40 to 0.25) μatm) and reduced outgassing fluxes. In contrast, in low to mid latitude regions (Figure 3d,h), the thermal-driven increase in oceanic $pCO_{2,O}$ typically dominates the flux response during MHWs. Changes in alkalinity play a moderate role in the equatorial Pacific (Figure 3f) and equatorial Atlantic (Figure 3g). However, in all other regions, both alkalinity and salinity changes play a negligible role.

It is important to note that a potential limitation of the Taylor decomposition is the assumption of linearity as we know that the functions governing air-sea CO_2 flux are nonlinear. To check whether this limitation has an impact on our attribution of the drivers we compare the sum of the Taylor decomposition terms with the calculated flux and driver anomalies. In particular for the air-sea CO_2 flux changes (grey bar versus horizontal black lines in Figures 2 and 3), there are slight discrepancies: the Taylor decomposition tends to overestimate the flux anomalies in the North Atlantic (Figure 2b), equatorial Pacific (Figure 2f) and low-mid latitudes (Figure 2d,h), while underestimating anomalies in the North Pacific (Figure 2b). Thus, this limitation may alter our quantitative assessment of the drivers, but we maintain confidence in the robustness of the qualitative findings of the drivers.

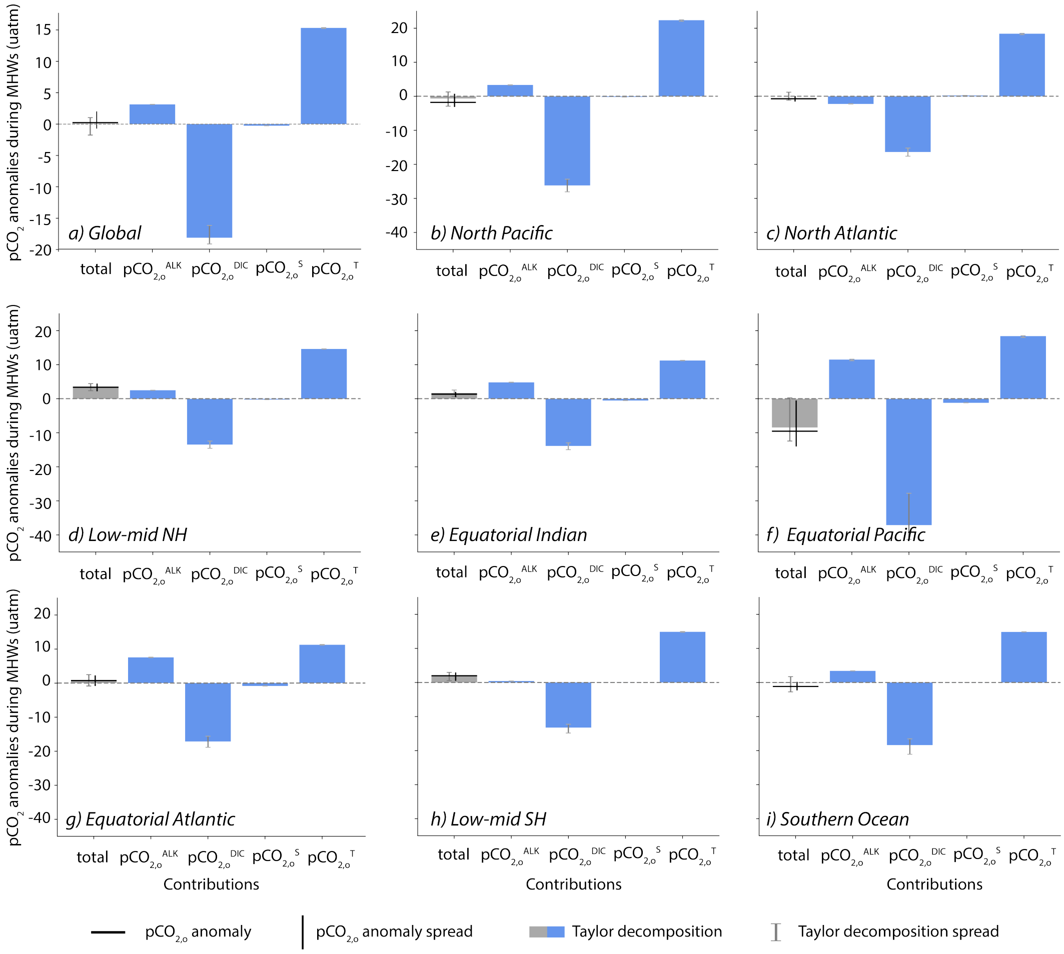

Figure 3. Global and regional drivers of oceanic $pCO_{2,o}$ anomalies during MHWs over the 1990-2019 period across all observation-based products. The results are shown for regions where all six observation-based $pCO_{2,o}$ products have data. The blue bars represent the average contribution of each $pCO_{2,o}$ term to the total $pCO_{2,o}$ anomalies during MHWs with grey error bars representing the min-max spread across the 30 observation-based data products. The grey bar is the sum of all the contribution terms. For comparison, the horizontal black line is the averaged observation-based product oceanic $pCO_{2,o}$ anomalies during MHWs, and the black error lines represent the min-max spread across the 30 observation-based data products. A positive total contribution indicates an increase in oceanic $pCO_{2,o}$.

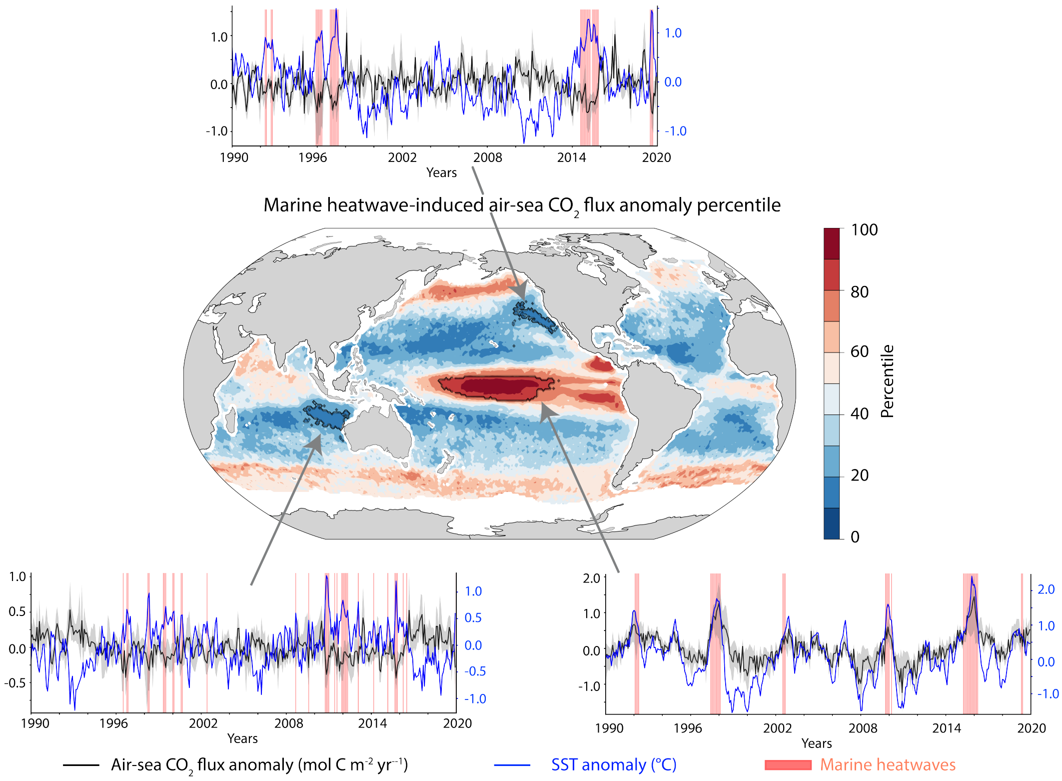

Figure 4. Global pattern of the percentile associated with the mean air-sea CO_2 flux anomalies averaged over all MHW months, compared to the local empirical distribution of monthly detrended air-sea CO_2 flux anomalies from 1990-2019. For three specific 'extreme' regions where the percentile of air-sea CO_2 flux anomalies exceeds 80% or falls below 20% of the average regional distribution, the time series of the mean monthly detrended air-sea CO_2 flux anomalies across all data products, detrended sea surface temperature anomalies (blue lines) and identified MHW events (red shading) are shown. The black shading shows the min-max range across all 30 air-sea CO_2 flux data products.

3.3 Importance of MHW-induced CO_2 flux anomalies within its natural variability

Next, we examine the importance of CO_2 flux anomalies induced by MHWs in the broader context of natural variations in air-sea CO_2 exchange. Our aim is to determine whether strong CO_2 flux anomalies are primarily attributable to MHWs or if these events play a minor role in explaining the substantial variations in air-sea CO_2 fluxes.

Across much of the global ocean, particularly in the low-to-mid latitudes, Southern Ocean and Atlantic Ocean, the mean air-sea CO_2 flux anomalies during MHWs do not surpass the 80% or 20% percentile of average background flux variations (Figure 4). This suggests that MHWs do not distinctly induce strong anomalies in air-sea CO_2 fluxes in these regions. However, areas experiencing very strong positive or negative flux anomalies during MHWs relative to the natural variations in air-sea CO_2 fluxes are the equatorial Pacific, Northeast Pacific, and eastern Indian Ocean (regions depicted in Figure 4).

The pronounced CO_2 flux response during MHWs is particularly strong in the central equatorial Pacific, where mean CO_2 flux anomalies exceed the 80th percentile of the CO_2 flux distribution. These periods of extreme anomalous CO_2 uptake often coincide with

El Niño events in these regions (Oliver et al., 2019; Holbrook et al., 2019; Le Grix et al., 2021). For example, the strongest El Niño events in 2015/2016 and of 1997/98 align with the most extreme anomalous oceanic CO_2 uptake observed in the past 30 years in this region. Similarly, in the eastern North Pacific, we observe very strong anomalous outgassing occurring during MHWs, falling below the 20th percentile of the regional distribution. These strong outgassing events also often coincide with El Niño events.

In the eastern Indian Ocean, MHWs induce strong anomalous CO_2 outgassing (below the 20th percentile). For example, the MHWs in 2010/11 and 2015/16 off the northwest coast of Australia triggered extreme anomalous outgassing. In the northern North Pacific, substantial anomalous CO_2 uptake occurs during several MHW events in the earlier part of the time period, but the spread across data products is large.

4 Discussion and conclusions

We show that the global oceanic uptake of CO_2 is only slightly reduced during MHWs. However, regionally, MHWs can have a substantial impact on air-sea CO_2 fluxes. We find the flux responses to be mainly driven by changes in the partial pressure of CO_2 in the ocean, which are a net result of two competing mechanisms during MHWs: a thermal effect and a non-thermal DIC effect. In regions where decreases in oceanic $pCO_{2,O}$ reduce CO_2 outgassing (e.g., equatorial Pacific) or increase CO_2 uptake (North Pacific and Southern Ocean), the primary driver is a reduction in DIC. In contrast, in regions (e.g., mid-latitudes) where increases in oceanic $pCO_{2,O}$ diminish the air-sea CO_2 uptake, temperature rises are the main driving factor for changes in oceanic $pCO_{2,O}$. Furthermore, while air-sea CO_2 flux anomalies triggered by MHWs can stand out as extreme anomalies in some regions such as in parts of the tropics and the Northeastern Pacific, MHW events are not necessarily important drivers for strong air-sea CO_2 flux anomalies in many other regions.

Our results align with Mignot et al. (2022) in the equatorial Pacific, where DIC outweighs the temperature effect on oceanic $pCO_{2,O}$, resulting in a comparable reduction in outgassing (-31% in our study vs. 40% in Mignot et al. (2022)). The agreement is not surprising given that the analysis here is based on similar (though more) $CO_{2,O}$ products as used in Mignot et al. (2022)). Additionally, the additional constraint of focusing on 'persistent' MHWs in Mignot et al. (2022) is not needed in this region, since long-lasting El Niño driven MHW are prevalent there (Holbrook et al., 2019). Our results suggest that Mignot et al. (2022)'s findings regarding anomalous outgassing in the mid-latitude North Pacific during MHWs, attributed to warmer temperatures, can be extrapolated to low-to-mid latitude CO_2 uptake regions in both hemispheres. This flux response resembles seasonal flux variations in these regions, where during summertime, the thermally driven increase in oceanic $pCO_{2,O}$ is slightly counteracted by the decrease in oceanic $pCO_{2,O}$ due to increased stratification which brings less DIC to the surface, but ultimately the thermal effect prevails (Fay & McKinley, 2017; Takahashi et al., 2002). In the high latitudes, MHWs induce different responses, with regions such as the Southern Ocean and North Pacific experiencing enhanced carbon uptake, while others like the North Atlantic show attenuated uptake. Nevertheless, findings of this study suggest that in high latitudes, the $pCO_{2,O}$ response during MHWs is primarily driven by the non-thermal DIC effect. Furthermore, this DIC-driven $pCO_{2,O}$ response controls the flux response in the Southern Ocean and the North Pacific, consistent with Duke et al. (2023).

Our study indicates a comparatively small impact of MHWs on air-sea CO_2 variability, contrasting with the substantial impact of land heat waves on regional carbon fluxes (Reichstein et al., 2013; Frank et al., 2015). Terrestrial heat waves (and droughts), such as the European events in 2003, 2010 and 2018, significantly reduced regional vegetation productivity due to various factors like soil moisture deficits, heat stress, and increased fire activity, leading to a net CO_2 uptake reduction (Ciais et al., 2005), though the regional drivers and responses may be complex (Bastos et al., 2020). Our study shows that MHWs in certain ocean regions can induce extreme CO_2 flux changes (e.g., Western Australia 2011 MHW; Arias-Ortiz et al. (2018)), but these events are more exceptional than common.

Furthermore, we show that observation-based products generally agree with each other regarding the direction of air-sea CO_2 flux anomalies during MHWs in the low-mid latitudes and the equatorial Pacific. However, discrepancies arise in higher latitudes, notably the North Pacific and Southern Ocean, possibly due to limited observational data in these regions. The lack of comprehensive data underscores the need for improved observation-based datasets and sustained data collection (Dong et al., 2024). Such data will enable us to enhance our understanding of how air-sea CO_2 fluxes respond to climate extremes, particularly in crucial carbon sink areas. Moreover, future research shall explore the influence of seasons and background states on the air-sea CO_2-flux response to MHWs, as the dominant effect (thermal versus non-thermal) on oceanic $pCO_{2,O}$ may depend on the season (Burger & Frölicher, 2023) and the background state — the latter highly relevant under future climate change.

Open Research Section

The observational-based air-sea CO_2 flux data products are available under https://zenodo.org/records/5482547, the NOAA OISSTv2.1 data under https://www.ncei.noaa.gov/products/optimum-interpolation-sst, the Hadley Centre EN4.2.2 salinity data under https://www.metoffice.gov.uk/hadobs/en4/download-en4-2-2.html, and the phosphate and silicate World Atlas 2018 data under https://www.ncei.noaa.gov/access/worl ocean-atlas-2018/. The analysis scripts used in this study will be available under a Zenodo repository link.

Acknowledgments

This work has received funding from the Swiss National Science Foundation (PP00P2_198897) and was supported by AtlantECO (project number: 862923) as well as TipESM and ClimTIP, which are both funded by the European Union. Views and opinions expressed are however those of the author(s) only and do not necessarily reflect those of the European Union or the European Climate, Infrastructure and Environment Executive Agency (CINEA). Neither the European Union nor the granting authority can be held responsible for them. We also thank the CSCS Swiss National Supercomputing Centre for computing resources.

References

Arias-Ortiz, A., Serrano, O., Masqué, P., Lavery, P., Mueller, U., Kendrick, G., … Duarte, C. (2018, April). A marine heatwave drives massive losses from the world's largest seagrass carbon stocks. *Nature Climate Change*, *8*(4), 338–344. doi: 10.1038/s41558-018-0096-y

Bakker, D. C. E., Pfeil, B., Landa, C. S., Metzl, N., O'Brien, K. M., Olsen, A., … Xu, S. (2016). A multi-decade record of high-quality fCO_2 data in version 3 of the surface ocean CO_2 atlas (SOCAT). *Earth System Science Data*, *8*(2), 383–413. doi: https://doi.org/10.5194/essd-8-383-2016

Bastos, A., Ciais, P., Friedlingstein, P., Sitch, S., Pongratz, J., Fan, L., … Zaehle, S. (2020). Direct and seasonal legacy effects of the 2018 heat wave and drought on european ecosystem productivity. *Science Advances*, *6*(24), eaba2724. doi: https://doi.org/10.1126/sciadv.aba2724

Bian, C., Jing, Z., Wang, H., Wu, L., Chen, Z., Gan, B., & Yang, H. (2023). Oceanic mesoscale eddies as crucial drivers of global marine heatwaves. *Nature Communications*, *14*(1), 2970. doi: https://doi.org/10.1038/s41467-023-38811-z

Boyer, T. P., García, H. E., Locarnini, R. A., Zweng, M. M., Mishonov, A. V., Reagan, J. R., ... Smolyar, I. V. (2018). *World Ocean Atlas 2018. [Volume 4: Dissolved Inorganic Nutrients (phosphate, nitrate and nitrate+nitrite, silicate).* NOAA National Centers for Environmental Information. Dataset. Retrieved from `https://www.ncei.noaa.gov/archive/accession/NCEI-WOA18`

Burger, F. A., & Frölicher, T. L. (2023). Drivers of Surface Ocean Acidity Extremes in an Earth System Model. *Global Biogeochemical Cycles*, *37*(9), e2023GB007785. doi: https://doi.org/10.1029/2023GB007785

Carter, B. R., Feely, R. A., Williams, N. L., Dickson, A. G., Fong, M. B., & Takeshita, Y. (2018). Updated methods for global locally interpolated estimation of alkalinity, pH, and nitrate. *Limnology and Oceanography: Methods*, *16*(2), 119–131. doi: https://doi.org/10.1002/lom3.10232

Cheung, W. W. L., & Frölicher, T. L. (2020). Marine heatwaves exacerbate climate change impacts for fsheries in the northeast Pacific. *Scientific Reports*, *10*. doi: https://doi.org/10.1038/s41598-020-63650-z

Cheung, W. W. L., Frölicher, T. L., Lam, V. W. Y., Oyinlola, M. A., Reygondeau, G., Sumaila, U. R., ... Wabnitz, C. C. C. (2021). Marine high temperature extremes amplify the impacts of climate change on fish and fisheries. *Science Advances*, *7*(40). doi: https://doi.org/10.1126/sciadv.abh0895

Ciais, P., Viovy, N., Reichstein, M., Seufert, G., & Matteucci, G. (2005). Europe-wide reduction in primary productivity caused by the heat and drought in 2003. *Nature*, *437*, 529-533. doi: https://doi.org/10.1038/nature03972

Collins, M., Sutherland, M., Bouwer, L., Cheong, S.-M., Frölicher, T., Jacot Des Combes, H., ... Tibig, L. (2019). *Extremes, abrupt changes and managing risk. in: IPCC special report on the ocean and cryosphere in a changing climate* (Tech. Rep.). Cambridge University Press.

Dong, Y., Bakker, D. C. E., & Landschützer, P. (2024). Accuracy of ocean CO_2 uptake estimates at a risk by a reduction in the data collection. *Geophysical Research Letters*, *51*(9), e2024GL108502. doi: https://doi.org/10.1029/2024GL108502

Duke, P. J., Hamme, R. C., Ianson, D., Landschützer, P., Ahmed, M. M. M., Swart, N. C., & Covert, P. A. (2023). Estimating marine carbon uptake in the northeast Pacific using a neural network approach. *Biogeosciences*, *20*, 3919–3941. doi: https://doi.org/10.5194/egusphere-2023-870

Edwing, K., Wu, Z., Lu, W., Li, X., Cai, W.-J., & Yan, X.-H. (2024). Impact of marine heatwaves on air-sea CO_2 flux along the US east coast. *Geophysical Research Letters*, *51*(1). doi: https://doi.org/10.1029/2023GL105363

Fay, A. R., Gregor, L., Landschützer, P., McKinley, G. A., Gruber, N., Gehlen, M., ... Zeng, J. (2021). Seaflux: Harmonization of air-sea CO_2 fluxes from surface pCO_2 data products using a standardized approach. *Earth System Science Data*, *13*(10), 4693 – 4710. doi: https://doi.org/10.5194/essd-13-4693-2021

Fay, A. R., & McKinley, G. A. (2017). Correlations of surface ocean $p\mathrm{CO}_2$ to satellite chlorophyll on monthly to interannual timescales. *Global Biogeochemical Cycles*, *31*(3), 436–455. doi: https://doi.org/10.1002/2016GB005563

Frank, D., Reichstein, M., Bahn, M., Thonicke, K., Frank, D., Mahecha, M. D., ... Zscheischler, J. (2015). Effects of climate extremes on the terrestrial carbon cycle: concepts, processes and potential future impacts. *Global Change Biology*, *21*(8), 2861-2880. doi: https://doi.org/10.1111/gcb.12916

Friedlingstein, P., O'Sullivan, M., Jones, M. W., Andrew, R. M., Bakker, D. C. E., Hauck, J., ... Zheng, B. (2023). Global carbon budget 2023. *Earth System Science Data*, *15*(12), 5301–5369. doi: 10.5194/essd-15-5301-2023

Frölicher, T. L., Fischer, E. M., & Gruber, N. (2018). Marine heatwaves under global warming. *Nature*, *560*, 360–364. doi: https://doi.org/10.1038/s41586-018-0383-9

Frölicher, T. L., & Laufkötter, C. (2018). Emerging risks from marine heat waves. *Nature Communications*, *9*. doi: https://doi.org/10.1038/s41467-018-03163-6

Garcia, H. E., Weathers, C. R., K. andPaver, Smolyar, I., Boyer, T. P., Locarnini, R. A., Zweng, M. M., … Reagan, J. R. (2019). *World Ocean Atlas 2018, volume 4: Dissolved inorganic nutrients (phosphate, nitrate and nitrate+nitrite, silicate).* A. Mishonov Technical Ed.; NOAA Atlas NESDIS 84.

Gattuso, J.-P., Magnan, A., Billé, R., Cheung, W. W. L., Howes, E. L., Joos, F., … Turley, C. (2015). Contrasting futures for ocean and society from different anthropogenic CO_2 emissions scenarios. *Science*, *349*(6243), aac4722. doi: https://doi.org/10.1126/science.aac4722

Good, S. A., Martin, M. J., & Rayner, N. A. (2013). EN4: Quality controlled ocean temperature and salinity profiles and monthly objective analyses with uncertainty estimates. *Journal of Geophysical Research: Oceans*, *118*(12), 6704-6716. doi: https://doi.org/10.1002/2013JC009067

Gray, A. R., Johnson, K. S., Bushinsky, S. M., Riser, S. C., Russell, J. L., Talley, L. D., … Sarmiento, J. L. (2018). Autonomous biogeochemical floats detect significant carbon dioxide outgassing in the high-latitude southern ocean. *Geophysical Research Letters*, *45*(17), 9049-9057. doi: https://doi.org/10.1029/2018GL078013

Hobday, A. J., Alexander, L. V., Perkins, S. E., Smale, D. A., Straub, S. C., Oliver, E. C., … Wernberg, T. (2016). A hierarchical approach to defining marine heatwaves. *Progress in Oceanography*, *141*, 227-238. doi: https://doi.org/10.1016/j.pocean.2015.12.014

Holbrook, N., Scannell, H. A., Gupta, A. S., Benthuysen, J. A., Feng, M., Oliver, E. C. J., … Wernberg, T. (2019). A global assessment of marine heatwaves and their drivers. *Nature Communications*, *10*, 2624. doi: https://doi.org/10.1038/s41467-019-10206-z

Huang, B., Liu, C., Banzon, V., Freeman, E., Graham, G., Hankins, B., … Zhang, H. M. (2021). Improvements of the daily optimum interpolation sea surface temperature (DOISST), version 2.1. *Journal of Climate*, *34*(8). doi: https://doi.org/10.1175/JCLI-D-20-0166.1

Hughes, T., Kerry, J., Alvarez-Noriega, M., Álvarez Romero, J., Anderson, K., Baird, A., … Wilson, S. (2017). Global warming and recurrent mass bleaching of corals. *Nature*, *543*, 373–377. doi: https://doi.org/10.1038/nature21707

Humphreys, M. P., Lewis, E. R., Sharp, J. D., & Pierrot, D. (2022). PyCO2SYS v1.8: marine carbonate system calculations in Python. *Geoscientific Model Development*, *15*(1), 15–43. doi: https://doi.org/10.5194/gmd-15-15-2022

IPCC. (2021). Summary for Policymakers. In V. Masson-Delmotte et al. (Eds.), *Climate Change 2021: The Physical Science Basis. Contribution of Working Group I to the Sixth Assessment Report of the Intergovernmental Panel on Climate Change* (pp. 3–32). Cambridge, United Kingdom and New York, NY, USA: Cambridge University Press. doi: https://doi.org/10.1017/9781009157896.001

Joos, F., Plattner, G.-K., Stocker, T. F., Marchal, O., & Schmittner, A. (1999). Global Warming and Marine Carbon Cycle Feedbacks on Future Atmospheric CO_2. *Science*, *284*(5413), 464-467. doi: https://doi.org/10.1126/science.284.5413.464

Landschützer, P., Gruber, N., & Bakker, D. C. E. (2016). Decadal variations and trends of the global ocean carbon sink. *Global Biogeochemical Cycles*, *30*(10), 1396-1417. doi: https://doi.org/10.1002/2015GB005359

Le Grix, N., Zscheischler, J., Laufkötter, C., Rousseaux, C. S., & Frölicher, T. L. (2021). Compound high-temperature and low-chlorophyll extremes in the ocean over the satellite period. *Biogeosciences*, *18*(6), 2119–2137. doi: https://doi.org/10.5194/bg-18-2119-2021

Mignot, A., von Schuckmann, K., Landschützer, P., Gasparin, F., van Gennip, S., Perruche, C., … Amm, T. (2022). Decrease in air-sea CO_2 fluxes caused by persistent marine heatwaves. *Nature Communications*, *13*, 4300. doi:

https://doi.org/10.1038/s41467-022-31983-0

Oliver, E. C. J., Benthuysen, J. A., Darmaraki, S., Donat, M. G., Hobday, A. J., Holbrook, N. J., … Gupta, A. S. (2021). Marine heatwaves. *Annual Review of Marine Science*, *13*, 313–342. doi: https://doi.org/10.1146/annurev-marine-032720-095144

Oliver, E. C. J., Burrows, M. T., Donat, M. G., Sen Gupta, A., Alexander, L. V., Perkins-Kirkpatrick, S. E., … Smale, D. A. (2019). Projected marine heatwaves in the 21st century and the potential for ecological impact. *Frontiers in Marine Science*, *6*. doi: https://doi.org/10.3389/fmars.2019.00734

Oliver, E. C. J., Donat, M. G., Burrows, M. T., Moore, P. J., Smale, D. A., Alexander, L. V., … Wernberg, T. (2018). Longer and more frequent marine heatwaves over the past century. *Nature Communications*, *9*, 1–12. doi: https://doi.org/10.1038/s41467-018-03732-9

Orr, J. C., & Epitalon, J.-M. (2015). Improved routines to model the ocean carbonate system: mocsy 2.0. *Geoscientific Model Development*, *8*, 485–499. doi: https://doi.org/10.5194/gmd-8-485-2015

Pearce, A. F., & Feng, M. (2013). The rise and fall of the “marine heat wave” off western australia during the summer of 2010/2011. *Journal of Marine Systems*, *111-112*, 139-156. doi: https://doi.org/10.1016/j.jmarsys.2012.10.009

Reichstein, M., Bahn, M., Philippe Ciais and, D. F., Mahecha, M. D., Seneviratne, S. I., Zscheischler, J., … Wattenbach, M. (2013). Climate extremes and the carbon cycle. *Nature*(500), 287—295. doi: https://doi.org/10.1038/nature12350

Smale, D. A., Wernberg, T., Oliver, E. C. J., Thomsen, M., Harvey, B. P., Straub, S. C., … Moore, P. J. (2019). Marine heatwaves threaten global biodiversity and the provision of ecosystem services. *Nature Climate Change*, *9*, 306–312. doi: https://doi.org/10.1038/s41558-019-0412-1

Takahashi, T., Sutherland, S. C., Sweeney, C., Poisson, A., Metzl, N., Tilbrook, B., … Nojiri, Y. (2002). Global sea–air CO_2 flux based on climatological surface ocean $p\mathrm{CO}_2$, and seasonal biological and temperature effects. *Deep Sea Research Part II: Topical Studies in Oceanography*, *49*(9), 1601–1622. doi: https://doi.org/10.1016/S0967-0645(02)00003-6

Vogt, L., Burger, F. A., Griffies, S. M., & Frölicher, T. L. (2022). Local drivers of marine heatwaves: A global analysis with an Earth System Model. *Frontiers in Climate*, *4*. doi: https://doi.org/10.3389/fclim.2022.847995

Wanninkhof, R. (1992). Relationship between wind speed and gas exchange over the ocean revisited. *Journal of Geophysical Research*, *97*(C5), 7373–7382. doi: https://doi.org/10.4319/lom.2014.12.351

Wilks, D. S. (2019). Statistical methods in the atmospheric sciences (fourth edition. In *Statistical methods in the atmospheric sciences (fourth edition)* (Fourth Edition ed., p. 771-805). Elsevier. doi: https://doi.org/10.1016/B978-0-12-815823-4.09992-2